ISSN 1855-9913 Journal of the Laser and Health Academy
Vol. 2020, No.1; www.laserandhealth.com

Smooth-Surfacing of Soft Tissues Using Thermal Er:YAG Laser Pulse Sequences

(Submitted for presentation at the 3rd LA&HA Super Symposium 2020)

Matjaz Lukac[1], Anze Zorman,[2] Blaz Tasic,[3] Nejc Lukac[4]
[1]Institut Jozef Stefan, Jamova 39, 1000 Ljubljana, Slovenia
[2]Medilase Dermatology &Laser Center, Tbilisijska 59, 1000 Ljubljana, Slovenia
[3]Fotona d.o.o., Stegne 7, 1000 Ljubljana, Slovenia
[4]University of Ljubljana, Faculty of Mechanical Engineering, Askerceva 6, 1000 Ljubljana, Slovenia

I. INTRODUCTION

Ablative skin resurfacing by Er:YAG lasers has proven to be an effective and reproducible method for treating wrinkles [1-4]. In erbium laser procedures, it is the tissue's water content, not its pigment that plays the role of an absorbing chromophore. The laser induced temperature elevation ΔT is thus not limited to a particular pigment, such as melanin or hemoglobin, but to the superficially irradiated tissue layer with its thickness determined by the laser's optical penetration depth (δ) and the subsequent thermal diffusion [5, 6]. Very roughly, the elevated temperature lasts for the combined duration of the laser pulse and subsequent conductive cooling, which is for typical Er:YAG single laser pulse durations on the order of one millisecond.

The Er:YAG laser treatments consist of heating the superficial tissue up to the maximally achievable temperature defined by the ablation temperature T_{abl} where tissue ablation starts, as a result of micro-explosions of overheated tissue water within the elastic skin tissue [6]. Since the water contained within the confined solid tissue cannot expand freely, the ablation temperature is not at the boiling temperature of water under atmospheric pressure of about 100 ^{0}C but at a much higher temperature of $T_{abl} \approx 250\ ^0$C [6, 7].

Resurfacing with the Er:YAG laser has been of particular interest since it allows for the so-called "cold" ablation with minimal thermal damage below the ablation front [4, 8]. This may be somewhat surprising considering the high superficial temperatures encountered during ablation. Namely, the heating of tissue is accompanied by the chemical process of protein denaturation as a result of the cellular exposure to the increased temperature [9]. The tissue damage is typically calculated using the Arrhenius damage integral Ω calculated over the time of the thermal exposure [9-12], according to which the tissue injury grows exponentially with the elevated temperature T, and linearly with the time of exposure Δt. The tissue damage is often characterized by a critical (i.e., damage threshold) temperature (T_{crit}), representing the temperature at which the concentration of the undamaged tissue is reduced by a factor of e. According to the Arrhenius model of skin damage developed by Henriques and Moritz [11, 12], based on measurements at longer exposures, the critical temperature for the exposure durations encountered during Er:YAG laser treatments would be around 70 ^{0}C, significantly below the ablation temperature.

Recently [7], it was pointed out that the above discrepancy can be explained by noting that during measurements performed at extremely short exposure times ($\Delta t < 10$ ms), the critical temperatures have been found to be significantly higher than what would be expected from the standard single process Arrhenius model [13 -16]. Using a VHS (Variable Heat Shock) model where the tissue thermal response was modeled with two interacting biochemical processes, defining the cell viability at very long and very short exposure times [16, 17], it was shown that for typical Er:YAG laser treatment parameters the critical temperature is above T_{abl} [7]. This was attributed to the uniquely short thermal exposure times, facilitated by the uniquely short optical penetration depth of the Er:YAG laser wavelength (λ = 2.940 nm) of δ = 1-3 μm in soft tissues. The resulting extremely large thermal gradient between the superficially optically heated tissue and the underlying tissue leads to a very short temperature decay time that combined with a typical Er:YAG laser pulse duration results in a total duration of the thermal exposure on the order of 1 millisecond.

It has also been suggested that the extremely short high-temperature, yet safe Er:YAG thermal pulses imposed on the epitelium involve an additional intense heat shocking regenerative mechanism that is complementary to the conventional deep thermal stimulation of fibroblasts [7]. This additional, superficial mechanism of action for regenerating epithelial and deeper lying connective tissues was proposed to be based on triggering stimulating signal transduction processes for transcription factor activation, gene expression and fibroblast growth, thus leading to new collagen and extracellular matrix formation [17-23].

While ablative laser resurfacing procedures have been found to be extremely effective, a major disadvantage is the erosion of large surfaces, which

necessitates a recuperation period of 1 to 2 weeks. There are also potential risks of infections, scarring or hyper- and hypo-pigmentation [24-26]. For this reason, it has been proposed to utilize the unique superficial absorption characteristics of Er:YAG also for less invasive non-ablative treatments [3, 5, 27, 28]. As opposed to ablative procedures, the main mechanism of action of standard non-ablative procedures is based on selective deep thermal damage followed by new collagen formation. With the Er:YAG laser, however, the mechanism of action potentially involves also the proposed superficial heat shock triggering [7, 27, 28].

In non-ablative treatments, the depth of tissue's thermal response is determined by the amount of heat which can be delivered to the tissue in a non-ablative manner. The maximal coagulation depth is thus limited by the maximal surface temperature $T_{max} = T_{abl}$, and related maximal laser pulse fluence F_{abl} (in J/cm^2), above which ablation starts [6]. The ablation threshold fluence can be increased by using longer laser pulses during which the delivered heat has more time to diffuse deeper into the tissue, effectively reducing surface temperature and thus increasing F_{abl} [6, 8]. However, since the existing Er:YAG laser technology limits single pulse durations to below several milliseconds, this limits the maximal coagulation depths which can be achieved with single pulses to maximally up to several tens of micrometers. For this reason, Er:YAG laser non-ablative procedures are typically carried out with longer-duration sequences of multiple laser pulses [29-31].

Many of the published studies of non-ablative, thermal treatments with Er:YAG laser pulse sequences have been made at relatively high sequence fluences, close to or slightly above the ablation threshold [29, 30-34]. This resulted in a significant damage to the epidermis, and in most cases also in subsequent removal of the damaged epidermis, making the treatments "delayed ablative".

In this study, we explored a different modality of non-ablative Er:YAG treatments, a "smooth-surfacing", where the cumulative fluence is set to be not only below the ablation threshold but also below the pain threshold for treatments without anesthesia, or at most with topical anesthesia. The technique involves delivering laser energy in 0.1-10 s long "SMOOTH" mode sequences, each consisting of several consecutive sub-ablative sub-millisecond Er:YAG laser pulses [3, 5, 27, 28]. During the SMOOTH mode sequence, the laser-generated heat is effectively "pumped" by means of heat diffusion away from the epithelia, several hundred microns deep into the connective tissue.

The temperature and tissue response characteristics during smooth-resurfacing were analyzed numerically for a broad range of treatment parameters. The tissue response was calculated using the two-process VHS model, in order to take into account the fast superficial temperature changes during individual laser pulses, and slower cumulative heat deposition during the over-all laser pulse sequence. Pain thresholds were measured during treatments with and without topical anesthesia, for different pulse sequence settings. Using the obtained pain threshold values, we evaluated the tissue response for a wide range of sub-surfacing laser parameters.

II. MATERIALS AND METHODS

a) Physical model of tissue smooth-surfacing

A numerical model was applied of the physical process of non-ablative sub-surfacing of soft tissues as originally developed to study thermo-mechanical ablation with mid-IR lasers. The details of the model are described in [6], and will not be repeated here.

In the model, a single wavelength (λ) pulsed laser radiation is delivered to the surface of the treated tissue with a total pulse fluence F (in J/cm^2). The tissue is modeled as a water-containing homogeneous media characterized by a single absorption coefficient of $k = 1/\delta$, for the delivered laser wavelength λ. For simplicity, a square-shaped laser pulse with duration t_L, was assumed. Since the focus of our study was on the Er:YAG laser wavelength with a short penetration depth, the effects of the scattering of the laser light within the tissue were not included. Similarly, it was taken that the laser spot size is much larger than the penetration depth (δ) and therefore the diffusion of dissipated heat was treated in one dimension using a finite-difference scheme. In all our calculations, we used the physical parameters of the irradiated media as published in [6].

The model was applied to calculate temporal and spatial temperature profiles for single pulses and as well for 0.1- 10 s long SMOOTH mode sequences, each consisting of several (N = 2 - 36) consecutive sub-ablative sub-millisecond Er:YAG laser pulses at pulse separation times of t_{ser} = 10 – 125 ms. The effective durations of the modeled pulse sequences, defined as the "long pulse" irradiation times $t_{ir} = N$ x t_{ser} was in the range of t_{ir} = 20- 4500 ms.

Since we were interested in determining at what single pulse and cumulative pulse sequence fluences the

laser-tissue interaction starts being ablative, the model also included the microscopic physical model of the ablative micro-explosion process, which combines the thermodynamic behavior of tissue water with the elastic response of the solid tissue components [6].

b) Chemical model of tissue sub-surfacing

The physical process of thermodynamically heating the tissue during a laser irradiation is accompanied by the chemical process of protein denaturation as a result of the cellular exposure to the increased temperature [17]. The tissue damage is calculated using the Arrhenius damage integral Ω calculated over the time of the thermal exposure [17,22,23]:

$$\Omega = A \exp(-E/RT)\, \Delta t \ . \quad (1)$$

Here, A is the frequency factor, i.e. the damage rate (in s^{-1}), E is the activation energy [in J/kmol], and R is the gas constant (R= 8.31 10^3 J/kmol K). The damage integral defines the probability (p) for tissue damage response according to:

$$p = 1- \exp(-\Omega_i) \ . \quad (2)$$

Similarly, the critical (i.e., damage threshold) temperature (T_{crit}), depends on the thermal exposure time as:

$$T_{crit} = E/(R \ln(A\, \Delta t) \ . \quad (3)$$

Studies of tissue damage dynamics have shown that for extremely short and long exposure times, cell viability cannot be described by a single biochemical process using a single Arrhenius damage integral according to Eq. 1 [11-16]. At extremely short exposure times the critical temperature has been measured to be significantly higher than what is predicted by the standard Arrhenius damage model assuming a single biochemical process [11-12].

Since during Er:YAG laser pulsing the tissue's over-all thermal exposure transitions from intense, extremely short exposure periods to moderate-temperature long exposure periods, a recently published VHS (Variable Heat Shock) response model [7], was used to evaluate the tissue damage Ω from the calculated temporal and spatial temperature profiles. The VHS model assumes that the critical temperature can be expressed as a combined effect of two biochemical processes that dominate cell survival characteristics at very short (below ≈ 5 ms) and very long (above ≈ 500 ms) exposure times. The details of the VHS damage integration method are described in [7], and will not be repeated here. The short pulse exposure process 1 and the long pulse exposure process 2 were characterized by Arrhenius parameters A_1 = (4.7 ± 1.4) x 10^{89} s^{-1} and E_1 = (5.67 ± 0.11) x 10^7 $Jkmol^{-1}$, and A_2 = (1.45± 0.15) x 10^4 s^{-1} and E_2 = (1.03± 0.03) x 10^7 $Jkmol^{-1}$, correspondingly [7].

c) Skin surface temperature measurement

The Er:YAG laser used for the measurement was Dynamis SP (manufactured by Fotona d.o.o.). In order to verify the physical model, a test measurement of the skin surface temperature evolution during and following a single Er:YAG laser pulse was made and compared with the results of the model. The measurement was made on the dorsal skin located between the thumb and the index finger of one of the authors. The temperature temporal profile for a single laser pulse was obtained with a high-speed thermal camera (FLIR A6750 SLS manufactured by FLIR Systems, Inc) at a frame rate of 4000 Hz.

Longer duration temperature profiles were measured on abdominal skin using a thermal camera (ThermaCAM P45, manufactured by FLIR Systems, USA) with a frame rate of 50 Hz.

c) Pain threshold measurement

In order to determine heat pain thresholds during non-ablative sub-surfacing for different pulse sequence parameters, we recorded discomfort threshold laser fluences of 15 patients during skin tightening treatments of the abdomen, either with or without topical anesthesia (EMLA). The pain threshold fluence F_p was obtained by increasing the V-SMOOTH fluence until the patients reported the treatment to be unpleasant.

The Er:YAG laser used in the measurement was Dynamis SP (manufactured by Fotona d.o.o.) operating in a V-SMOOTH pulse mode delivering laser pulse sequences with adjustable pulse separation time t_{ser} from 25 ms to 125 ms, and adjustable number of pulses from N = 6 to 36. The laser pulse duration was t_L = 0.3 ms. The laser energy was delivered to the tissue using a T-Runner scanning handpiece (manufactured by Fotona d.o.o.) with a single spot size of 9 mm, scanned over a reduced scanning area of ≈ 4 cm^2.

III. RESULTS

a) Single pulse temperature profile

Figure 1 shows the measured single pulse temporal temperature profile at the skin surface, together with the simulated temperature profile during and following pulsed Er:YAG laser irradiation [51]. A special high-speed thermal camera (FLIR A6750 SLS, manufactured by FLIR Systems, USA) at a fast frame rate of 4000 Hz was used to detect the extremely fast temperature evolution during and following a single Er:YAG laser pulse generated by a Dynamis SP laser system equipped with a 5-mm full-beam R11 handpiece (both manufactured by Fotona d.o.o., Slovenia). The laser pulse fluence of F_p = 0.80 J/cm^2 was set to be just below the low fluence ablation threshold $F_p = F_{abl1}$ = 0.88 J/cm^2.

Since for this measurement, the dorsal skin area was cleaned with alcohol prior to irradiation, the measured skin hydration level was low, with skin hydration level of H ≈ 8% . For higher skin hydration levels, the ablation threshold would be higher. It is also to be noted that the low fluence ablation threshold F_{abl1} is different from the high fluence ablation threshold F_{abl}. At low fluences the ablation threshold is reached only at the end of a laser pulse. The ablation effect is very small but can be detected by the slight whitening of the tissue surface. At higher fluences, the ablation temperature is reached almost immediately after the on-set of the laser pulse, and the ablation process takes place during the whole duration of the laser pulse. In this regime, the ablation depth depends approximately linearly on the laser pulse fluence, and the high fluence ablation threshold F_{abl} is represented by the fluence where the linear relationship crosses the zero-ablation depth value; and has been determined for skin to be in the fluence range of 1.6 -2.2 J/cm^2.

As can be seen from Fig. 1, the temperature pulse consists of the temperature ramp-up heating phase during which the temperature reaches its maximal value (T_{max}), and of the temperature ramp-down cooling phase during which the temperature returns back to its initial temperature T_0. The heating phase lasts approximately for the duration of the laser intensity pulse (t_L), while the cooling phase is determined predominantly by the rate of the heat flow away from the heated tissue volume. The exponential decay time τ of the tissue temperature is equal to τ = 2.0 msec, with t_{max} = 1.54 msec.

The optical penetration depth of Er:YAG in pure water (H = 100%) is equal to $\delta_0 \approx 0.8$ μm. Since the absorption of Er:YAG in dry tissue is relatively low, the penetration depth δ for a tissue with a certain water content H can be calculated from $\delta = 100\% \times \delta_0/H$. Assuming that that following the heating phase the tissue's surface temperature decays exponentially from T_{max} with a decay time $\tau \approx (1/D)\, d_{heat}^2$, where $D \approx 0.11$ mm^2 s^{-1} is the thermal diffusivity of the tissue, and d_{heat} represents the depth to which the tissue had been heated by the end of the laser pulse, then d_{heat} can be approximated by $d_{heat} \approx \delta + d_{pulse}$, where δ is the optical penetration depth and $d_{pulse} \approx (D.\, t_{laser})^{1/2}$ is the depth to which the deposited heat diffuses from the optical penetration depth deeper into the tissue during the duration of the laser pulse (t_L). The following very approximate equation is then obtained for estimating the decay time: $\tau \approx (1/D) \times (\delta + (D \times t_L)^{1/2})^2$. Taking H = 8%, we obtain $\tau = 2.17$ msec, in good agreement with the measured decay time of 2 msec.

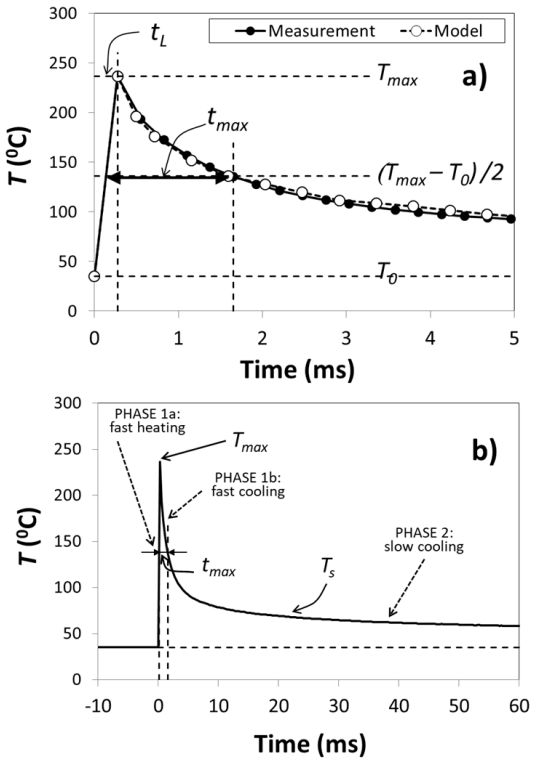

Fig. 1: a) Simulated and measured thermal pulse as generated by a t_L = 0.27 ms long Er:YAG laser pulse with fluence of F_L = 0.8 J/cm^2 [51]. The time t_{max} represents the FWHM width of the temperature pulse. The ablation threshold temperature T_{abl} at the ablation fluence of F_p = 0.88 J/cm^2 can be obtained from the measured maximal temperature of T_{max} = 240 ^{0}C at F_p = 0.8 J/cm^2, to be equal to $T_{abl} \approx 256$ ^{0}C, in good agreement with $T_{abl} \approx 252$ ^{0}C from ref. [6]. b) The same temperature evolution shown on a longer scale. The temperature pulse consists of a sharp high-peak temperature pulse (Phase 1) followed by a longer temperature decay tail (Phase 2).

The ablation threshold temperature T_{abl} at the ablation fluence of F_p = 0.88 J/cm^2 can be obtained from the measured maximal temperature of T_{max} = 240 ^{0}C at F_p = 0.8 J/cm^2, to be equal to $T_{abl} \approx 256$ ^{0}C, in good agreement with $T_{abl} \approx 252$ ^{0}C from ref. [6].

For fluences below the ablation threshold, the maximal tissue temperature T_{max} grows linearly with fluence at a single pulse temperature slope of $\eta_1 = \Delta T_{max}/F_L$, where $\Delta T_{max} = T_{max} - T_0$. The maximal temperature increases with laser fluence until the ablation threshold fluence F_{abl1} is reached, at which point the maximal temperature achieves the ablation ("boiling") temperature T_{abl}. Figure 2 presents the influence of single pulse duration t_L on the temperature slope η_1 and ablation threshold fluence F_{abl1}. The initial temperature was taken to be equal to T_0 = 30 ^{0}C.

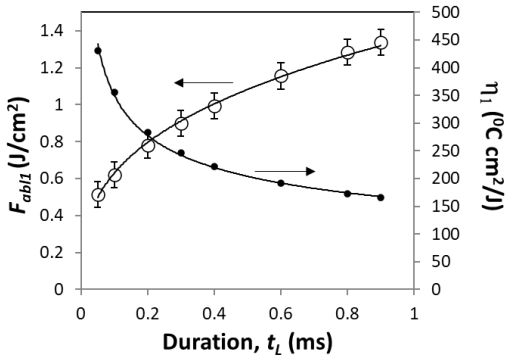

Fig. 2: Dependence on the Er:YAG single pulse duration (t_L) of the measured single pulse ablation threshold fluence (F_{abl1}) and correspondingly calculated single pulse temperature slope ($\eta_1 = \Delta T_{max}/F$). The full lines are fits according to Eqs. 4 and 5. The low fluence ablation threshold fluence at t_L = 0.27 msec is equal to F_{abl1} = 0.88 J/cm². It is to be noted that these measurements were made on a very dry skin ($H_i \approx 8\%$). For higher skin hydration levels, the ablation thresholds would be higher, and the temperature slopes would be lower.

Fits to data presented in Fig. 2 give approximate dependences of the single pulse temperature slope η_1 (in ^{0}Ccm²/J) and single pulse ablation threshold fluence F_{abl1} (in J/cm²), on the single laser pulse duration t_L (in ms) as follows:

$$\eta_1 (t_L) \approx 162\ t_L^{-1/3}\ , \qquad (4)$$

and

$$F_{abl1}\ (t_L) \approx 1.37\ t_L^{1/3}\ . \qquad (5)$$

For fluences above F_{abl1}, the maximal temperature remains fixed at T_{abl} by means of micro-explosions, similarly to the case of boiling water that keeps its temperature at about 100 ^{0}C regardless of the heating power. Using our numerical model, the soft tissue ablation temperature is calculated to be $T_{abl} \approx 256$ ^{0}C, regardless of pulse duration, in good agreement with other reports [6, 35, 36].

b) Multiple pulse temperature profile

Figure 3a presents a calculated temperature profile at the tissue surface, as calculated for a N = 6 pulse sequence at pulse separation period t_{ser} = 50 ms, cumulative fluence of $F = N$ x F_L = 4.4 J/cm², and t_L = 300 μs.

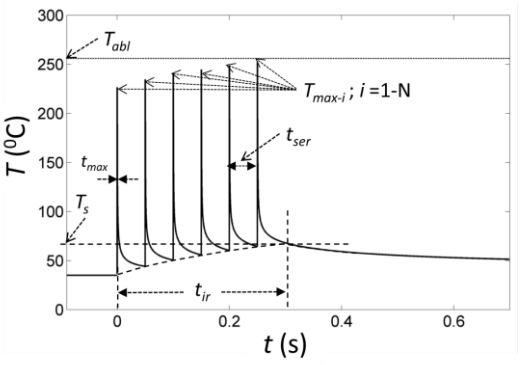

Fig. 3a: Simulated temperature profile during and following a laser pulse train consisting of N = 6 pulses with duration t_{ir} = t_{laser} = 300 ms. T_s denotes the maximal baseline temperature T_{max}.

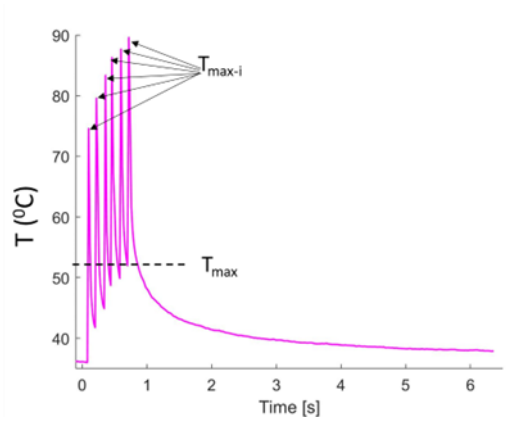

Fig. 3b: Exemplary temporal evolution of the skin surface temperature during a SMOOTH pulse sequence of 6 pulses with overall duration t_{ir} = t_{laser} = 750 ms. T_{max} denotes the maximal baseline temperature, as measured with a thermal camera FAST M3K, manufactured by Telops, Inc., Canada.

The multiple pulse train sequence results in N high temperature peaks which rapidly relax by fast thermal diffusion driven by the large temperature gradient over the short optical absorption length. On the longer scale, the overall effect of the long pulse train is to heat up the tissue surface at $t = t_{ir}$ to approximately the same temperature as if the laser energy was delivered to the tissue with a total laser fluence of $F = N$ x F_L , in a single long square shaped pulse with a duration $t_{ir} = N$ x t_{ser}. This final, longer persisting surface temperature is in Fig. 5a represented by the "long pulse" temperature T_s.

Figure 3b presents a measured temperature profile at the tissue surface, as calculated for a N = 6 pulse sequence at pulse separation period t_{ser} = 125 ms, and t_{ir} = 750 ms, as measured with a thermal camera FAST M3K, manufactured by Telops, Inc., Canada

The multiple pulse train sequence results in N high temperature peaks which rapidly relax by fast thermal diffusion driven by the large temperature gradient over the short optical absorption length. On the longer scale, the overall effect of the long pulse train is to heat up the tissue surface at $t = t_{ir}$ to approximately the same temperature as if the laser energy was delivered to the tissue with a total laser fluence of $F = N$ x F_L , in a single long square shaped pulse with a duration $t_{ir} = N$ x t_{ser}. This final, longer persisting surface temperature is in Fig. 3a represented by the "long pulse" temperature T_s.

The calculations show that the long pulse temperature T_s (i.e., T_{max}) depends approximately linearly on the total delivered fluence F, with the long pulse temperature slope defined by $\eta_2 = \Delta T_s/F$, where $\Delta T_s = T_s - T_0$. The slope depends predominantly on the long pulse duration (t_{ir}) while the dependence on the single pulse duration or on the number of pulses N is relatively small (See Fig. 4).

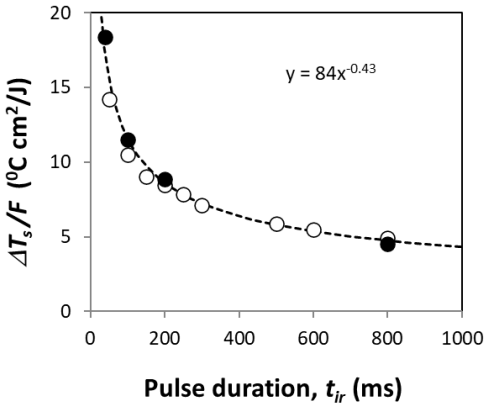

Fig. 4: Dependence of the full beam long pulse temperature slope η_2 on the long pulse duration, t_{ir}. Open circles represent the slopes for a N = 6 train of t_L = 300 μs pulses, and full circles represent the slopes for N = 4 train of t_L = 100 μs pulses. The dashed line represents a fit to the calculated values.

The resulting temperature increase as a function of the full beam fluence (handpiece R11) is for different long pulse durations depicted in Figure 5a. Shorter long pulse durations result in significantly higher temperatures.

Figure 5b shows the dependence of the long pulse temperature slope η_2 on the long pulse duration, t_{ir}, as obtained from measurements presented in Fig. 5a. A fit to data points shown in Fig. 5b gives the following dependence of the long pulse temperature slope $\Delta T_s/F$ (with ΔT_s in ^{0}C, and F in J/cm^2) on the long pulse duration t_{ir} (in ms) (R^2 = 0.96):

$$\eta_2 (t_{ir}) \approx 84 \; t_{ir}^{-0.43} . \quad (6)$$

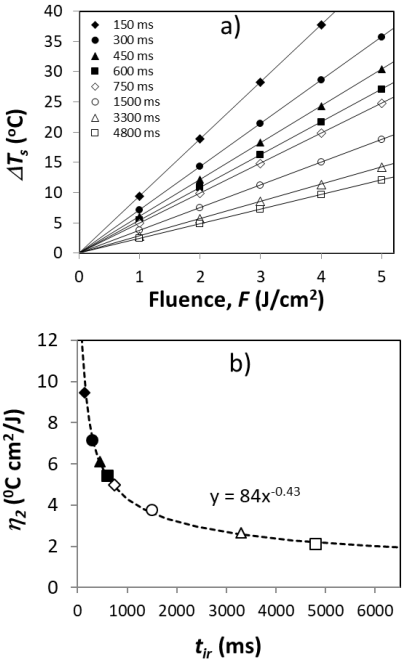

Fig. 5: a) Dependence of the full (R11) beam long pulse temperature increase on the cumulative fluence for different long pulse durations t_{ir}. b) Dependence of the long pulse temperature slope $\eta_2 = \Delta T_s/F$ on the long pulse duration, t_{ir}. The dashed line represents a fit to the measured values.

The resulting temperature increase as a function of the patterned beam fluence (handpiece PS03/PS03X) is for different long pulse durations depicted in Figure 6a. Figure 5b shows the dependence of the long pulse temperature slope η_2 on the long pulse duration, t_{ir}, as obtained from measurements presented in Fig. 6a. A fit to data points shown in Fig. 6b gives the following dependence of the long pulse temperature slope $\Delta T_s/F$ (with ΔT_s in ^{0}C, and F in J/cm^2) on the long pulse duration t_{ir} (in ms) (R^2 = 0.96):

$$\eta_2 (t_{ir}) \approx 28 \; t_{ir}^{-0.43} . \quad (7)$$

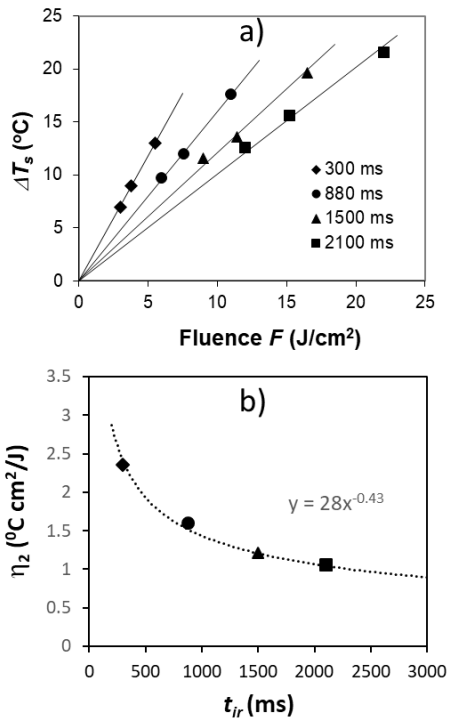

Fig. 6: a) Dependence of the patterned (PS03/PS03X) beam long pulse temperature increase on the cumulative fluence for different long pulse durations t_{ir}. b) Dependence of the long pulse temperature slope $\eta_2 = \Delta T_s/F$ on the long pulse duration, t_{ir}. The dotted line represents a fit to the measured values.

The ablation threshold is reached when the maximal temperature T_{max} (N) of the last pulse in the sequence with long pulse duration t_{ir} results in the ablation temperature T_{abl}. Assuming that all laser pulses (i = 1-N) in the sequence have the same fluence F_i, then ablation starts where ΔT_s (N-1) + $\eta_1 F_i = \Delta T_{abl} = 256\ ^0$C – T_0 = 221 ^{0}C, where ΔT_s (N-1) is the long pulse temperature elevation for the pulse sequence with N-1 pulses, i.e., with the long pulse duration of t_{ir} (N-1)/N. Using Eqs. The pulse sequence ablation threshold fluence F_{thr} = N F_i (in J/cm²) can then be calculated from:

$$F_{thr} = N\,\Delta T_{abl}\,/(\eta_1\,(t_L) + (N\text{-}1)\,\eta_2\,(t_{ir}(N\text{-}1)/N) \qquad (8)$$

Using Eq. 8, Fig. 7 shows the calculated dependence of the pulse sequence ablation threshold F_{thr} on long pulse duration t_{ir}, for several values of t_L and N.

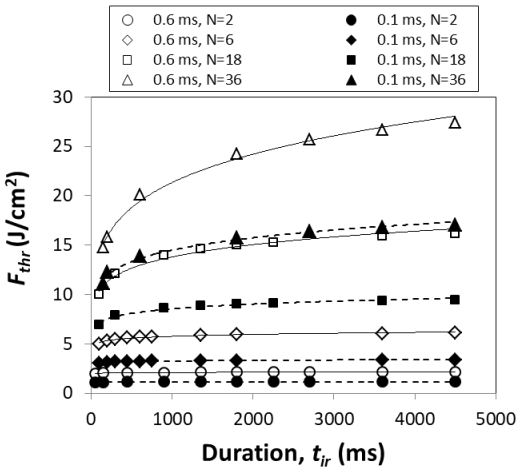

Fig. 7: Ablation threshold cumulative fluence for sequences of N = 2, 6, 18 and 36, for two single pulse durations, t_L = 0.1 and 0.6 ms, as a function of the long pulse duration t_{ir}. The lines are guide to the eye, not supported by theory.

Figure 7 shows that the ablation threshold depends more strongly on N and t_L, than on t_{ir}, especially for longer t_{ir}.

d) Pain threshold

Figure 8 shows measured pain threshold fluences F_p as measured without topical anesthesia on 15 patients for four long pulse settings: i) N = 6, t_{ir} = 150 ms; ii) N = 30, t_{ir} = 3750 ms; iii) N = 36, t_{ir} = 3600 ms; and iv) N = 36, t_{ir} = 4500 ms.

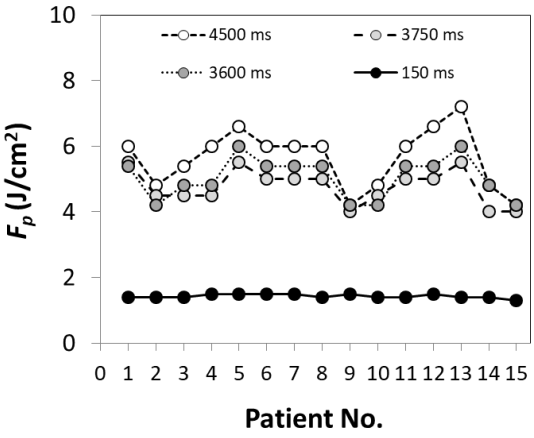

Fig. 8: Measured pain threshold fluences F_p for four pulse sequence durations: 150, 3600, 3750 and 4500 ms, as reported by 15 patients. No topical anesthesia was used.

As can be seen from Fig. 8, while pain thresholds vary from patient to patient, the pain threshold fluence is generally higher for longer pulse duration t_{ir}.

This can also be seen in Fig. 9 which shows the difference in reported pain threshold fluences for two pulse sequence durations (150 ms and 4500 ms) depending on whether a topical anesthesia (EMLA cream) was used or not.

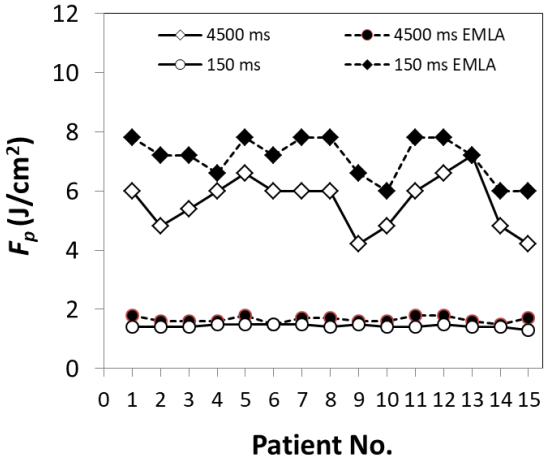

Fig. 9: Measured pain threshold fluences F_p for pulse sequence durations 150 ms and 4500 ms, depending on whether a topical anesthesia was used or not.

On average, topical anesthesia increases pain threshold fluence for 16 % and 26 %, for the 150 ms and 4500 ms irradiation time, respectively.

The pain threshold temperatures as calculated from the measured pain threshold fluences (Figs. 8 and 9 using Eq. 4, are shown in Fig. 10. The pain threshold temperature is approximately constant over the studied range of long pulse irradiation times, and is on the average equal to $\Delta\underline{T}_p$ = 13.2 ^{0}C for treatments without anesthesia, and $\Delta\underline{T}_{pa}$ = 15.6 ^{0}C for treatments with topical anesthesia.

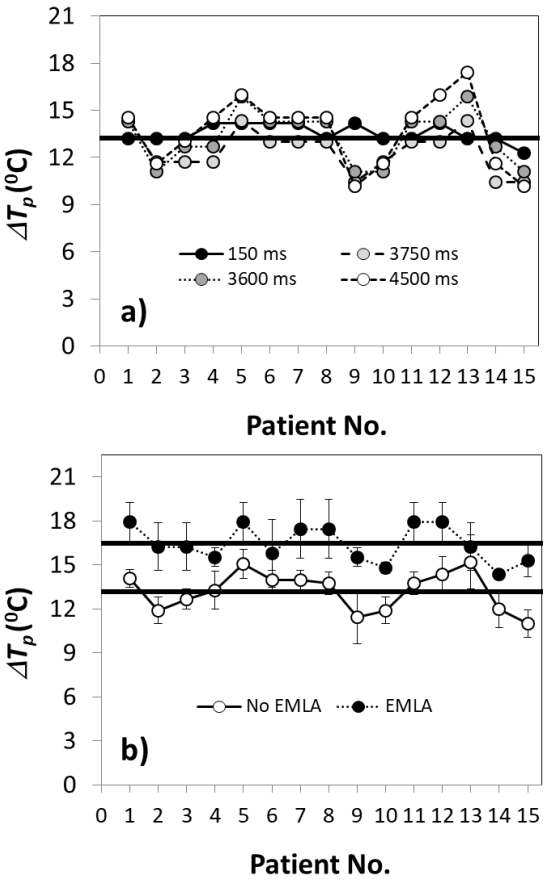

Fig. 10: a) Pain threshold temperatures for treatments without anesthesia, for irradiation times 150, 3600, 3750 and 4500 ms. The thick line represents the average pain threshold temperature for without EMLA, ΔT_p = 13.2 ^{0}C b) Average pain threshold temperatures for treatments without (averaged over 150, 3600, 3750 and 4500 ms data; open circles) and with topical anesthesia (averaged over 150 and 4500 ms data; full circles). Full lines represent average pain threshold temperatures for treatments without anesthesia, ΔT_p = 13.2 ^{0}C, and with anesthesia, ΔT_{pa} = 16.5 ^{0}C.

Figure 11a shows the dependence of the average pain threshold fluence F_p on the irradiation time, and Fig. 10b depicts the averaged pain threshold temperatures for different long pulse irradiation times, both for treatments with and without topical anesthesia.

As can be seen from Fig.101 the pain threshold fluence is strongly dependent on t_{ir}, while the pain threshold temperature is approximately constant over a wide range of tested pulse durations.

In Fig. 11a), the dashed and full lines represent calculated pain thresholds using Eq. 1 for $\Delta\underline{T}_s = \Delta T_p$ = 13.2 ^{0}C and $\Delta\underline{T}_s = \Delta T_{pa}$ = 15.6 ^{0}C, respectively:

$$F_p \approx \Delta T_p/70\ t_{ir}^{-0.4}, \quad (9)$$

The fit of Eq. 9 to the pain data points is better than R^2 =0.98.

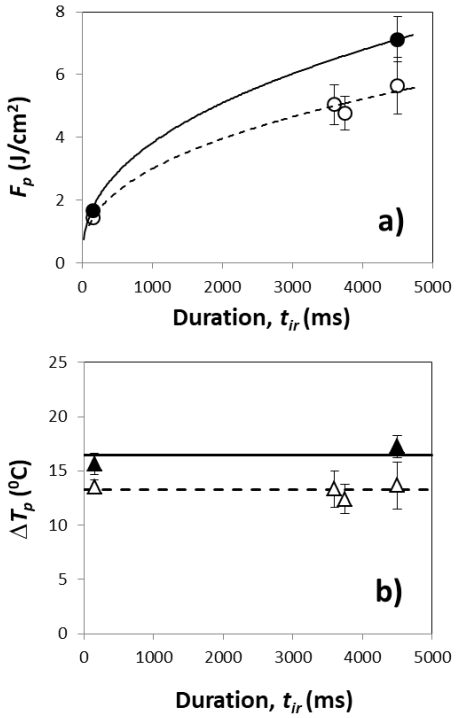

Fig. 11: Dependence of a) measured pain threshold fluences F_p; and b) calculated pain threshold temperatures, on irradiation time. Full and open symbols represent data for treatments with and without anesthesia, respectively. The represent pain threshold fluences as calculated according to Eq. 1 (Fig. 10a), and average pain threshold temperatures for treatments without (ΔT_p = 13.2 ^{0}C) (dashed line) and with anesthesia (ΔT_{pa}= 15.6 ^{0}C) (full line).

e) Tissue response

Finally, Fig. 12 shows the calculated coagulation depths z_c as a function of the long pulse duration t_{ir}, for three cumulative fluences F = 2.4, 4.8 and 7.2 J/cm². The tissue coagulation depth (z_c) was defined as the tissue depth above which the cell injury is larger than Ω = 0.5.

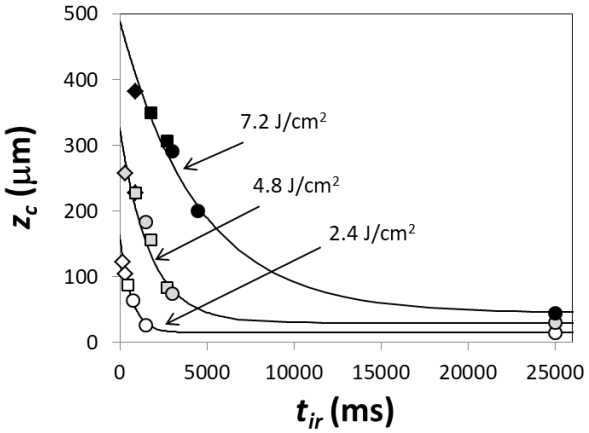

Fig. 12: Calculated coagulation depths, z_c for three cumulative fluences F = 2.4, 4.8 and 7.2 J/cm², as a function of the long pulse duration, t_{ir}. The calculations were made for pulse repetition periods t_{ser} = 25 ms (diamonds), 75 ms (squares) and 125 ms (circles). The lines are according to Eq. 9.

Our analysis shows that the dependence of z_c (in μm) on the irradiation time t_{ir} (in ms) and cumulative fluence F (in J/cm²) can be very roughly described by

$$z_c \approx F\,(6.25+61.75 \exp(-0.004\, t_{ir} / \tau)), \qquad (10)$$

where τ (in ms) = exp(-0.4 F). Note that this expression is not supported by a theory. However, as will be shown further below, it represents a useful relationship for optimizing otherwise complex sub-surfacing conditions.

IV. DISCUSSION

Tissue sub-surfacing and resurfacing with Er:YAG lasers represents an extreme example of complex thermal exposure dynamics during which the exposure times transition from extremely short to moderately long durations. This can be seen from Fig. 1b which shows that very roughly, the heat transfer dynamics upon single-pulsed Er:YAG laser irradiation can be divided into two phases, a high-temperature short duration phase and a moderate-temperature long duration phase.

During the first phase, the superficial tissue is for the duration of the Er:YAG laser pulse (t_L) initially directly heated within the optical absorption depth δ of the incoming laser light, followed by a rapid cooling driven by thermal diffusion, with a cooling rate $\tau_1 \approx \delta^2/D$. Here, D is the thermal diffusivity of the tissue (for skin D = 1.1 10^{-7} m²/s). Since the optical absorption depth of Er:YAG in soft tissues is only

several microns thick, and therefore the directly heated tissue volume is very small, this phase results in high peak temperatures T_{max}, and also in extremely short cooling times. The resulting, approximately triangularly shaped high peak temperature pulse (See Fig. 1) has a FWHM duration $t_{max} \approx t_L + \tau_1$, that is for typical Er:YAG laser pulse durations on the order of one millisecond. Therefore, during the first phase, the tissue is exposed to an intense thermal pulse with temperature T_{max} for the duration t_{max}, which is characterized by higher critical temperatures of the short exposure biochemical process. This explains why very high skin surface peak temperatures T_{max}, up to the ablation temperature of T_{abl} = 256 ^{0}C do not result in an irreversible tissue damage. The Arrhenius equation with parameters based on measurements at longer exposure times predicts damage integral $\Omega \geq 0.5$ already for temperatures above $T \approx 70$ ^{0}C.

The second phase of the thermal exposure starts when the surface cooling slows down after the effective conductive cooling of the interaction layer reduces the initially large temperature gradient. During this second phase, deeper tissue layers continue to get moderately heated, and remain at elevated temperatures for a significantly longer time (τ_2) which is on the order of seconds or longer. The second phase is thus governed by the long exposure biochemical process characterized by lower critical temperatures.

During a SMOOTH mode sequence, the above two-phased heat transfer dynamics is repeated during each individual pulse, with the temperature baseline progressively increasing following each pulse. Considering a common understanding that longer pulses result in larger coagulation depths [8], the decrease of the coagulation depth with pulse sequence duration (t_{ir}) as observed in Fig. 11, may appear surprising. However, for fluences below ablation threshold, the coagulation depth actually decreases with pulse duration. This is confirmed also by Fig. 2 which shows that shorter pulses result in a larger temperature slope η_1, and therefore for the same fluence also in higher peak temperatures T_{max}. Since tissue damage grows exponentially with elevated temperature (See Eq. 1), this leads to longer coagulation depths.

It is important to note that in a clinical setting, the maximal coagulation depth of pulse sequences is actually not limited by the ablation threshold fluence, F_{abl} (Fig. 7) but typically by the much lower pain threshold fluence F_p , which is higher for longer pulse sequence durations t_{ir}. (see Fig. 11a). This is because the measured pain threshold temperature elevation ΔT_p is approximately independent of the pulse sequence duration (See Fig. 11b), while longer sequence durations require higher fluences to achieve the same temperature elevation (see Fig. 11a).

For long exposures (several seconds) to elevated temperatures, the published pain thresholds for different body areas are in the range of 41-45 ^{0}C [37, 38,]. The heat pain threshold increases logarithmically towards shorter exposures, and is equal to ≈ 55 ^{0}C for ≈ 0.2 s and ≈ 70 ^{0}C for ≈ 0.05 s [39, 40]. The average pain threshold measured in this study (T_p ≈43 ^{0}C) is in good agreement with the published long exposure pain thresholds, which we attribute to the long temperature decay time τ_2 during the second phase of the Er:YAG laser induced heat dynamics, regardless of the duration of the pulse sequence. This also explains the observed approximately constant pain threshold temperature across a wide range of pulse sequence durations.

The combined effect of the coagulation depth decreasing with pulse duration (Fig. 12), and of the pain threshold fluence increasing with pulse duration (Fig. 10a), can be evaluated by combining the approximate relationships according to Eqs. 9 and 10. The results are presented in Fig. 13.

According to Fig. 13 the coagulation depth does not depend on the number of pulses N, and also not on the pulse repetition rate $1/t_{ser}$. This is providing that the pain threshold fluence (Eq. 5) is below ablation threshold fluence, a condition that can be fulfilled by using appropriately large N for the used single laser pulse duration t_L (See Fig. 7). Under this condition, the clinically achievable coagulation depth depends only on the pulse sequence duration, t_{ir}. This can be explained by considering that intense thermal pulsing caused by individual laser pulses gets "washed out" as the heat diffuses deeper into the tissue. The heat deeper within the tissue persists for a relatively long time, and therefore the deep coagulation the tissue response is governed by the long exposure Arrhenius damage process.

According to Fig. 13 the coagulation depth does not depend on the number of pulses N, and also not on the pulse repetition rate $1/t_{ser}$. This is providing that the pain threshold fluence is below ablation threshold fluence (Eq. 9), a condition that can be fulfilled by using appropriately large N for the used single laser pulse duration t_L (See Fig. 7). Under this condition, the clinically achievable coagulation depth depends only on the pulse sequence duration, t_{ir}. This can be explained by considering that intense thermal pulsing caused by individual laser pulses gets "washed out" as the heat diffuses deeper into the tissue. The heat deeper within the tissue persists for a relatively long time, and therefore the deep coagulation the tissue response is

governed by the long exposure Arrhenius damage process.

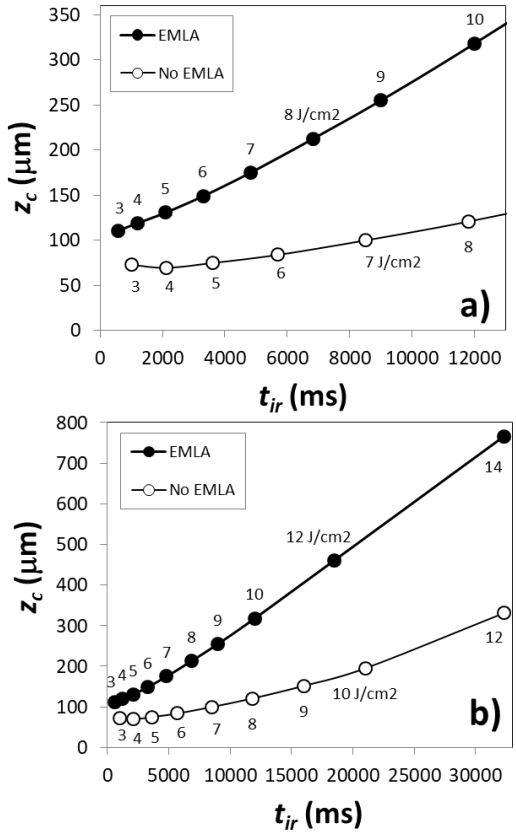

Fig. 13. Calculated dependence of the maximal coagulation depth, z_c on pulse sequence duration, for treatments with pain threshold fluences according to Eq. 5, for treatments without (full line) and with topical anesthesia (dashed line). The numbers by data points represent corresponding pain threshold fluences (in J/cm^2).

According to Fig. 12 the coagulation depth does not depend on the number of pulses N, and also not on the pulse repetition rate $1/t_{ser}$. This is providing that the pain threshold fluence (Eq. 9) is below ablation threshold fluence, a condition that can be fulfilled by using appropriately large N for the used single laser pulse duration t_L (See Fig. 7). Under this condition, the clinically achievable coagulation depth depends only on the pulse sequence duration, t_{ir}. This can be explained by considering that intense thermal pulsing caused by individual laser pulses gets "washed out" as the heat diffuses deeper into the tissue. The heat deeper within the tissue persists for a relatively long time, and therefore the deep coagulation the tissue response is governed by the long exposure Arrhenius damage process.

A question arises what effect if any does the intense thermal pulsing have on the tissue located very close to the surface. A simple calculation shows that during the intense first heating phase lasting for several milliseconds, the heat diffuses only up to 10 - 30 μm deep. While the baseline surface temperature gradually increases during the sequence, this thin superficial epidermal layer is subjected also to i = 1-N individual high temperature peaks, with an average temperature elevation within the layer of $\approx \Delta T_{maxi}/2$.

In order to evaluate the effect of intense thermal pulsing on the thin superficial layer, resulting from the short duration periods of high peak temperatures, we ignored the thermal damage caused by the gradual baseline temperature build-up during the longer times in-between the pulses. A probability-summation (PS) model of Menendez et al. [41, 42], was used where it is assumed that the response to each pulse of a multiple-pulse exposure is independent of the response to other pulses; that is, previous pulses do not "sensitize" the tissue to subsequent pulses. The probability p_i of thermal damage caused by each pulse i = 1- N is then calculated from

$$p_i = 1\text{- exp } (-\Omega_i) \ , \qquad (11)$$

where

$$\Omega_i = A_1 \exp(-E_1/R\ (T_{maxi}/2))\ \Delta t_{\text{eff}} \ . \qquad (12)$$

Here, A_1 and E_1 are the Arrhenius parameters for the short duration process, and $\Delta t_{\text{eff}} \approx 0.2$ ms was taken to represent the duration of an imaginary rectangular temperature pulse of a constant temperature $T_{maxi}/2$ which produces approximately the same amount of damage as the actual "triangularly" shaped temperature pulses [7].

By approximating the tissue response to each pulse by the same average single pulse probability $p_0 = \sum_i p_i/N$, then according to the PS model the cumulative probability $P(N)$ of inducing a thermal damage to the superficial layer during N pulses is calculated using (108):

$$P\ (N) = 1\text{- } (1\text{-}p)^N \ . \qquad (13)$$

This gives the cumulative superficial damage integral:

$$\Omega\ (N) = \text{Ln } (1/(1\text{-}P(N)) \quad . \qquad (14)$$

The calculated dependence of the cumulative superficial damage integral on the pulse sequence pulse duration, for treatments at pain threshold fluences is shown in Fig. 14.

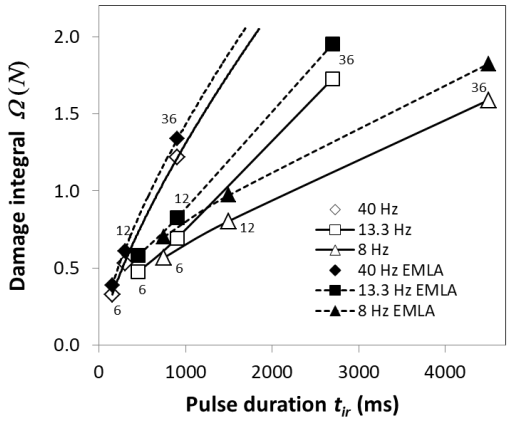

Fig. 14: Calculated dependence of the superficial damage integral on pulse sequence duration, for pain threshold fluences $F(t_{ir})$ according to Eq. 9. The numbers by the data points represent the number of pulses within a sequence, N.

As opposed to the deep thermal damage, the response of the superficial tissue layer to heat pulsing is strongly influenced by the pulse repetition rate $1/t_{ser}$, and by the number of pulses N. The superficial tissue response is higher for sequences with large number of pulses delivered at high repetition rates. Figure 14 also demonstrates that using topical anesthesia does not have as beneficial effect on superficial tissue response as on the deeper tissue coagulation (Fig. 13).

It should be also noted that it has been proposed that the delivery of extremely short Er:YAG thermal pulses to the epithelium involves an additional intense heat shocking regenerative mechanism that is complementary to the conventional direct slow thermal stimulation of fibroblasts. This additional, indirect mechanism of action for regenerating epithelial and deeper lying connective tissues was proposed to be based on triggering stimulating signal transduction processes for transcription factor activation, gene expression and fibroblast growth, thus leading to new collagen and extracellular matrix formation.

The above findings suggest two potential treatment modalities. When a deep tissue response is desired then long irradiation sequences using topical anesthesia are recommended, enabling delivery of high fluences without causing irreversible damage to the tissue or discomfort to the patient.

On the other hand, when only superficial skin laxity or tightening is to be addressed then moderate fluence-pulse sequences are recommended, using increased number of pulses and repetition rates. While topical anesthesia improves the effect it is not essential for this treatment.

And finally, when a practitioner desires to achieve both effects during the same treatment, then very long irradiation times delivered with a large number of pulses at high repetition rates are recommended.

The above findings may explain the reported safety and efficacy of the Smooth mode Er:YAG lasers when used for non-ablative skin tightening [27, 28, 43], thermotherapy of the vaginal wall to alleviate genitourinary syndromes of menopause [44-49], and for thermotherapy of snoring and sleep apnea [50].

NOTES

The authors acknowledge financial support from the state budget of the Ministry of Education, Science and Sport of Slovenia and the European Regional Development Fund (Project GOSTOP). The authors are affiliated also with Fotona d.o.o., Ljubljana, Slovenia.

REFERENCES

1. Alster TS. Clinical and histologic evaluation of six Erbium:YAG lasers for cutaneous resurfacing. Lasers Surg Med 1999; 24:87–92.
2. Khatri KA, Ross V, Grevelink JM (1999) Comparison of Erbium:YAG and Carbon Dioxide Lasers in Resurfacing of Facial Rhytides. Arch Dermatol 135(4): 391-397
3. Lukac M, Sult T, Sult R (2007) New Options and Treatment Strategies with the VSP Erbium YAG Aesthetics Lasers, J LA&HA, J Laser and Health Academy, Vol. 2007; No.1/2; www.laserandhealth.com
4. Cole RP, Widdowson D, Moore JC (2008) Outcome of erbium:yttrium aluminium garnet laser resurfacing treatments. Lasers Med Sci. 23(4):427-33.
5. Lukac M, Perhavec T, Nemes K, Ahcan U (2010) Ablation and Thermal Depths in VSP Er:YAG Laser Skin Resurfacing., J LA&HA, J Laser and Health Academy, Vol. 2010, No. 1; 56-71. www.laserandhealth.com
6. Majaron B, Plestenjak P, Lukac M (1999), Thermo-mechanical laser ablation of soft biological tissue: modeling the micro-explosions. Appl. Phys. B 69, 71–80
7. Lukac M, Lozar A, Perhavec T, Bajd F. (2019) Variable heat shock response model for medical laser procedures, Lasers Med Sci. 2019 Aug;34(6):1147-1158. doi: 10.1007/s10103-018-02704-1.
8. Majaron B, Sustercic D, Lukac M, Skaleric U, Funduk N (1998) Heat diffusion and debris screening in Er:YAG laser ablation of hard biological tissues. Appl Phys B 66:479-487.
9. Johnson FH, Eyring H, and Stover BJ (1974) The Theory of Rate Processes in Biology and Medicine. Wiley, New York.
10. Wright NT (2003) On a relationship between the Arrhenius parameters from thermal damage studies. Journal of biomechanical engineering 125(2):300–304.
11. Henriques FC, Moritz AR (1947) Studies of thermal injury, 1. The conduction of heat to and through skin and the temperature attained therein. A theoretical and an experimental investigation. A J Pathol 23:531–549
12. Moritz AR, Henriques FC (1947) Studies of thermal injury, 2. The relative importance of time and surface temperature in the causation of burns. A J Pathol 23:695–720
13. D. M. Simanovskii, M. A. Mackanos, A. R. Irani, C. E. O'Connell-Rodwell, C. H. Contag, H. A. Schwettman, and D. V. Palanker, Cellular tolerance to pulsed hyperthermia, Phys Rev E 74, 011915 (2006), doi: 10.1103/PhysRevE.74.011915.
14. D. Simanovskii, M. Sarkar, A. Irani, C. O'Connell-Rodwell, C. Contag, A. Schwettman, D. Palanker, Cellular tolerance to pulsed heating, Proc. of SPIE 5695, 254-259 (2005), doi: 10.1117/12.601774.
15. Pirnat S, Lukac M, Ihan A (2011) Thermal tolerance of E. faecalis

to pulsed heating in the millisecond range. Lasers Med Sci (2011) 26:229–237
16. J. Kampmeier, B. Radt, R. Birngruber, R. Brinkman, Thermal and Biomechanical Parameters of Porcine Cornea., Cornea 19, 355, 2000: 355-363.
17. Bourke CD et al (2015) Epidermal keratinocytes initiate wound healing and pro-inflammatory immune responses following percutaneous schistosome infection International Journal for Parasitology 45: 215–224
18. Pastar I et al (2014) Epithelialization in wound healing: A comprehensive review. Advances in Wound Care. 3(7): 445-464
19. Wojtowicz AM et al (2014) The importance of both fibroblasts and keratinocytes in a bilayered living cellular construct used in wound healing Wound Rep Reg 22: 246–255.
20. Capon A, Mordon S (2003) Can thermal lasers promote skin wound healing?. Am J Clin Dermatol 4 (1): 1-12
21. Mackanosa MA, Contag CH (2011) Pulse duration determines levels of Hsp70 induction in tissues following laser irradiation. J Biomed Opt 16(7), 078002 (July 2011)
22. Lubart R, Friedmann H, Lavie R, Baruchin A (2011) A novel explanation for the healing effect of the Er:YAG laser during skin rejuvenation. Journal of Cosmetic and Laser Therapy 13: 33–34
23. Lubart R, Kesler G, Lavie R, Friedmann H (2005) Er:YAG laser promotes gingival wound repair by photo-dissociating water molecules. Photomed Laser Surg. 2005 Aug;23(4):369-72.
24. Fitzpatrick RE, Goldman MP, Sotur NM, Type WD. Pulsed carbon dioxide laser resurfacing of photoaged skin. Arch Dermatol 1996;132:395–402.
25. Greve B, Raulin C. Professional errors caused by laser and IPL technology in dermatology and aesthetic medicine. Preventive strategies and case studies. Derm Surg 2001;28: 156–161.
26. 10. Nanni CA, Alster TS. Complications of carbon dioxide laser resurfacing. An evaluation of 500 patients. Dermatol Surg 1998;24:315–320.
27. Lukac M, Zorman A, Bajd F (2018) TightSculpting®: A Complete Minimally Invasive Body Contouring Solution; Part II: Tightening with FotonaSmooth® Technology. J LA&HA, J Laser and Health Academy, Vol. 2018, No. 1; 26-35. www.laserandhealth.com
28. Lukac M, Gaspar A, Bajd F (2018) Dual Tissue Regeneration: Non-Ablative Resurfacing of Soft Tissues with FotonaSmooth® Mode Er:YAG Laser. J LA&HA, J Laser and Health Academy, Vol. 2018, No. 1; 1-15. www.laserandhealth.com
29. Majaron B, Srinivas SM, Huang HL, Nelson JS (2000) Deep coagulation of dermal collagen with repetitive Er:YAG laser irradiation. Lasers Surg. Med. 26:215–222
30. Majaron B, Kelly KM, Park HB (2001) Er:YAG Laser Skin Resurfacing Using Repetitive Long-Pulse Exposure and Cryogen Spray Cooling: I. Histological Study Lasers in Surgery and Medicine 28:121-130
31. Majaron B, Verkruysse W, Nelson S (2001) Er:YAG Laser Skin Resurfacing Using Repetitive Long-Pulse Exposure and Cryogen Spray Cooling: II. Theoretical Analysis. Lasers in Surgery and Medicine 28:131-137
32. Kunzi-Rapp K, Dierickx CC, Cambier B, Drosner M.(2006) Minimally invasive skin rejuvenation with Erbium: YAG laser used in thermal mode. Lasers Surg Med. 2006 Dec;38(10):899-907.
33. Drnovsek Olup B, Beltram M, Pizem J (2004) Repetitive Er:YAG laser irradiation of human skin: A histological evaluation. Lasers in Surg Med 35:146–151
34. Ross EV et al (2002) Use of a novel Erbium laser in a Yucatan minipig: A study of residual thermal damage, ablation, and would healing as a function of pulse duration. Lasers Surg Med 30; 93-100 DOI 10.1002/lsm.10030.
35. Zweig AD, Frenz M, Romano V, Weber HP (1988): A comparative study of laser tissue interaction at 2.94 μm and 10.6 μm. Appl. Phys. B 47: 259-265
36. G.L. LeCarpentier, M. Motamedi, L.P.McMath, S. Rastegar, A.J.Welch (1993) Continuous wave laser ablation of tissue: analysis of thermal and mechanical events. IEEE Trans. Biomed. Eng. 40: 188 -200.
37. Defrin R et al (2006) Quantitative Somatosensory Testing of Warm and Heat-Pain Thresholds: The Effect of Body Region and Testing Method; Clin J Pain 22(2): 130-136.
38. Yarnitsky D, Sprecher E, Zaslansky R, Hemli JA (1995). Heat Pain Thresholds - Normative Data and Repeatability. Pain 1995; 60(3):329-332.
39. Defrin R et al (2002) Sensory determinants of pain; Brain 125:501-501.
40. Arendt-Nielsen L, Chen CAN (2003) Lasers and other thermal stimulators for activation of skin nociceptors in humans. Neurophysiol Clin; 33(6):259-268.
41. Menendez AR, Cheney FE, Zuclich JA, Crump P. Probability-summation model of multiple laser-exposure effects. Health Phys 65:523–528; 1993.
42. Brian J. Lund, David J. Lund, and Peter R. Edsall, Damage threshold from large retinal size repetitive-pulse laser exposures. 2014 Health Physics Society.292-299
43. Gaspar A (2013) Tightening of Facial Skin Using Intraoral 2940 nm Er:YAG SMOOTH Mode, J LA&HA - J Laser Health Acad 2013; 2013(2):17-20.
44. G.A. Lapii, A. Yu. Yakovleva, and A.I. Neimark (2017) Structural Reorganization of the Vaginal Mucosa in Stress Urinary Incontinence under Conditions of Er:YAG Laser Treatment, Bulletin of Experimental Biology and Medicine, Feb Vol.162, No.10:510-514.
45. A. Gaspar, H.Brandi, V. Gomez, D. Luque (2016) Efficacy of Erbium:YAG Laser Treatment Compared to Topical Estriol Treatment for Symptoms of Genitourinary Syndrome of Menopause, Laser Surg Med. 49(2):160-168. doi: 10.1002/lsm.22569.
46. Bezmenko A.A. et al. (2014) Morphological substantiation of applying the Er:YAG laser for the treatment of stress urinary incontinence in women, Journal of Obstetrics and Women Diseases, 63(3):21-25.
47. I.A. Kulikov, L.B. Spokoinyi, E.A. Gorbunova,.I.A. Apolikhina (2017) A Method For Photothermal Tissue Reconstruction Using ErYAG Laser Fotona in Modern Gynecology, Akusherstvo i Ginekologiya / Obstertics and Gynecology, (11): 160-167.
48. J.F. Bojanini B., A. M. Mejía C., Laser Treatment of Vaginal Atrophy in Post-menopause and Post-gynecological Cancer Patients, J Laser and Health Academy (2014) No.1, 65-71.
49. Gambacciani M. et al., Short term effect of Vaginal Erbium Laser on the Genitourinary Syndrome of Menopause, Minerva Ginecologica (2015).
50. Storchi IF, Parker S, Bovis F, Benedicenti S, Amaroli A (2018) Outpatient erbium:YAG (2940 nm) laser treatment for snoring: a prospective study on 40 patients. Lasers Med Sci, published online Jan 15, 2018.
51. Lukac N, Tasic Muc B, Lukac M (2020) High-Temperature Triggering of Soft-Tissue Regeneration by Er:YAG Laser, J LA&HA, J Laser and Health Academy, Vol. 2020, No. 1; S3.